In situ fabrication of layered double hydroxide film immobilizing gold nanoparticles in capillary microreactor for efficient catalytic carbonylation of glycerol

Qi Ming She, Jia Hui Liu, Cyril Aymonier, Chun Hui Zhou

▶ **To cite this version:**

Qi Ming She, Jia Hui Liu, Cyril Aymonier, Chun Hui Zhou. In situ fabrication of layered double hydroxide film immobilizing gold nanoparticles in capillary microreactor for efficient catalytic carbonylation of glycerol. Molecular Catalysis, 2021, 513, pp.111825. 10.1016/j.mcat.2021.111825 . hal-03339915

HAL Id: hal-03339915
https://hal.science/hal-03339915v1

Submitted on 9 Sep 2021

HAL is a multi-disciplinary open access archive for the deposit and dissemination of scientific research documents, whether they are published or not. The documents may come from teaching and research institutions in France or abroad, or from public or private research centers.

L'archive ouverte pluridisciplinaire **HAL**, est destinée au dépôt et à la diffusion de documents scientifiques de niveau recherche, publiés ou non, émanant des établissements d'enseignement et de recherche français ou étrangers, des laboratoires publics ou privés.

In situ fabrication of layered double hydroxide film immobilizing gold nanoparticles in capillary microreactor for efficient catalytic carbonylation of glycerol

Qi Ming She[ab] Jia Hui Liu[a] Cyril Aymonier[c] Chun Hui Zhou[ad]

[a] Research Group for Advanced Materials & Sustainable Catalysis (AMSC), State Key Laboratory Breeding Base of Green Chemistry-Synthesis Technology, Institute of Industrial Catalysis, College of Chemical Engineering, Zhejiang University of Technology, Hangzhou, 310014, China
[b] College of Chemistry and Chemical Engineering, Huangshan University, Huangshan, China
[c] CNRS, Univ. Bordeaux, Bordeaux INP, ICMCB, UMR 5026, F-33600 Pessac, France
[d] Qing Yang Institute for Industrial Minerals, Youhua, Qingyang, Chizhou, Anhui, 242804, China

Abstract

Microreactor is capable of intensifying catalytic reaction processes. The fabricating of catalytic film inside microchannels for catalytic reaction remains a challenge. Here we report a facile method for *in situ* fabrication of layered double hydroxide (LDH) film immobilizing gold nanoparticles in capillary microreactor. Through adjusting the reaction condition of *in situ* hydrothermal crystallization process and flow deposition process inside microchannel, film thickness, film morphology and Au loading of Au/LDH coating can be finely controlled. Such Au/LDH film inside microchannel exhibited good performance in catalytic carbonylation of glycerol with urea. The yield of glycerol carbonate reached 31.9% at flow rate of 10 μl/min, residence time of 6.62 min and reaction temperature of 413 K under atmospheric pressure. The maximum productivity of 3.78 $g \cdot h^{-1} \cdot g^{-1}$ was obtained at flow rate of 40 μl/min and residence time of 1.65 min under same reaction temperature and pressure. Continuously running the microreactor for 30 h proved the high stability of this catalytic film inside microchannels. This approach could be extended to fabricate other diatomic and triatomic metal LDH films immobilizing metal nanoparticles inside microchannels for heterogeneous catalysis.

1. Introduction

Over the past two decades, microreactors have received considerable attention in process intensification and chemical research [1], [2], [3]. A microreactor can be fabricated as a chip or a capillary tube that exhibiting certain advantages of high surface-to-volume ratio, excellent mass and heat transfer properties [4]. However, the direct deposition of a catalytic active phase to reach a sufficient level of activity is hindered by the insufficient geometric surface area of capillary microchannels [5]. Therefore, porous SiO_2 [6,7], porous TiO_2 [8,9], ZnO nanorods [10], polydopamine [11], zeolites [12], [13], [14] and MOFs [15,16] have been introduced in microreactors to achieve the homogeneous dispersion and immobilization of catalytic active components, and realize supra-equilibrium conversions, resulting in improved reaction efficiency and intensified production processes. Furthermore, drawbacks such as high-pressure drop [17] and poor catalyst contacting and wetting [18] in traditional micro packed-bed reactors can be averted in an inner-wall coated microreactor. The inner-wall coating of the microreactor can also serve as a protective layer to prevent the active nanoparticles from leaching and aggregation [19]. Such inner wall coated microreactor received significant interest for heterogeneous catalysis owing to their innerface as catalysts and attractive supports. In addition, with the catalyst coating on the innerwall, temperature gradients can be eliminated and higher catalytic activity can be achieved [20]. Dynamic gas displacement, sol-gel deposition, static *in situ* generation and flow generation method can be utilized to fabricate the aforementioned films on the innerface of microchannels. Among these methods, the static *in situ* generation method is the most convenient approach to achieve continuous and uniform coatings inside microchannels.

As a large family of two-dimensional (2D) anionic clay materials, layered double hydroxide (LDH) have the general formula of $[Me_{1-x}^{II}Me_x^{III}(OH)_2A_n^{x/n-} \cdot nH_2O]$ (Me(II) and Me(III) are metal cations and A denotes anions) [21,22]. LDH comprise of positively charged brucite-like layers with an interlayer region containing charge compensating anions and solvation molecules [23]. On account of their flexibilities in composition and lamellar in structure, LDH are widely used as catalysts [24,25], catalyst precursors [26], anion exchangers [27], CO_2 absorbents [28], bioactive nanocomposites [29], electroactive [30] and photoactive materials [30]. Among these applications of LDH, their role as catalysts or precursors for catalysis has been attracted considerable interest. For example, Mg-Al-LDH with supported Au nanoparticles was found catalytically active in oxidation of alcohols [31] and methanol [32], degradation of organic contaminants [33] and reduction of 4-Nitrophenol [34]. However, the utilization of powdered layered double hydroxide catalysts on an industrial scale

inevitably bring out many problems, such as difficult catalyst separation and high pressure drop. These hitches can be solved by fabricating them into robust macroscopic form. Immobilization of LDH films on a monolithic substrate have become an ideal solution for solving such problems [35]. However, comparing with powdered form, fabricating LDH into well-oriented continuous supported thin films or self-supporting membranes remains a challenge. More recently, there has been a growing number of publications focusing on exploring the potential of LDH film as catalytic layer or support for loading catalytically active components. Through *in situ* growth or physical deposition methods, various LDH films were successfully immobilized on silicon wafer [36], glass sheet [37], indium tin oxides glass [38], metal foils [15,39], carbon nanotubes [40], and other monolithic substrate [41] for biodiesel production [42, 43] and volatile organic compounds degradation [41,44]. Comparing with physical deposition, the *in situ* growth method leads to uniform films with strong adhesion between LDH crystals and substrate [37]. However, there is a surprising paucity of studies investigating immobilization of LDH films inside microchannels, especially capillary microreactors for catalytic application.

Glycerol is being regarded as an ideal renewable platform chemical [45,46]. Glycerol carbonylation with urea is a promising route to upgrade two readily available and cheap reactants in a simple process with an atom economy. Furthermore, the product glycerol carbonate (GLC) is also an important platform chemical [47], [48], [49], [50]. Au nanoparticles [51] and LDH catalysts [52] were proved to be catalytically active for this reaction. However, the utilization of such catalysts suffer from harsh reaction conditions such as negative operation pressure [53] or purge with inert gas [54]. Furthermore, our exploratory experiments have found that the carbonylation of glycerol with urea was difficult to operate under negative operation pressure, and the whole reaction solution is easy to boil, resulting in a large number of low boiling point by-products. Moreover, the separation of heterogeneous catalysts for these batch process needs filtration or centrifugation, that is energy and time consuming [55]. These complex post-treatment process can be avoided by coating the catalysts inside microchannels. So far, however, no previous study has investigated to enable LDH film as a catalytic coating in capillary microreactor for the continuous synthesis of GLC under mild conditions.

Inspired by the above-mentioned principles, a novel method was proposed for fabricating an inner wall coated fused silica capillary microreactor based on Au nanoparticles (NPs) immobilized in LDH film (named as Au/LDH film) for glycerol carbonylation with urea under mild conditions. To strengthen the mass transfer and ensure a proper flow distribution inside capillary, efforts have been laid on both fabrication of capillary microreactor and the coating of the catalytic layers inside capillary microchannel. In order to contrast and analyze, pristine LDH powder catalyst, Au/LDH powder catalyst with the same loading as Au/LDH film and the LDH film capillary microreactor without any Au NPs were also studied for the carbonylation of glycerol with urea. Such Au/LDH film coated capillary microreactor hold the potential to be a more sustainable technology for upgrading waste feedstock to added value chemicals. Hence, this contribution aimed to bring a new concept on enabling LDH to be used in microreactors, and thus more effective microreactors can be realized by extending the fabrication of other LDH film-coated microchannel loaded with different active components.

2. Experimental

2.1. Materials

Fused silica capillaries (outer diameter: 630 μm, inner diameter: 530 μm, length: 30 mm) were purchased from Hebei Yong Nian Rui Feng GC Instrument Corporation. Magnesium nitrate hexahydrate ($Mg(NO_3)_2{\cdot}6H_2O$), aluminium nitrate nonahydrate ($Al(NO_3)_3{\cdot}9H_2O$), urea, hydrochloric acid (HCl), sodium hydroxide (NaOH), and N,N-dimethylformamide (DMF) were obtained from Sinopharm Chemical Reagent Beijing Co. Ltd. Sodium borohydride ($NaBH_4$), Au chloride solution (Au 23.5–23.8 wt% in dilute HCl), and poly(vinyl alcohol) were supplied by Shanghai Aladdin Chemical Co. Ltd. The used deionized water (DI water) was home-made.

2.2. Preparation of LDH film microreactors

2.2.1. Pretreatment of fused silica capillary

The pretreatment process prevented the inner wall of the pristine capillary from exhibiting poor adhesion to the LDH film and insufficiently robust for catalytic application. Schematic illustration for the pretreatment of fused-silica capillary was depicted in Fig. S1. Firstly, the inner surface of the capillaries was rinsed with 1M NaOH solution for 1 h at a flow rate of 25 μL/min, then flushed with DI water at the same flow rate until the outlet liquid is neutral sequentially. Thereafter, 0.1 M HCl solution was pumped in capillaries at a set rate of 20 μL/min for 1 h, followed by washing with distilled water at the same flow rate until the outlet liquid is neutral, and then dried in an oven at 393 K. This procedure induced the breaking of silicon-oxygen bonds and the generation of silicon hydroxyls for enhancing surface activity and adsorption properties on

the inner surface of the capillaries. On this basis, the pretreatment process provides conducive surface properties for the subsequent growth of LDH crystallites.

2.2.2. Synthesis of LDH film on the inner wall of capillaries

The fused silica capillary after pretreatment was utilized as a microchannel substrate for the hydrothermal growth of LDH film inside. As shown in Fig. 1b, the *in situ* growth of LDH film was realized in a self-made device. Firstly, 0.84 g urea, 0.26 g $Mg(NO_3)_2{\cdot}6H_2O$ and 0.19 g $Al(NO_3)_3{\cdot}9H_2O$ were dissolved in 15 mL DI water to form a homogeneous precursor solution. Second, the precursor solution was injected into the microchannels of pretreated fused silica capillary at a set flow rate of 0.25 mL/h until the capillary was completely filled. Third, the capillary was sealed at the inlet and outlet and heating in a thermostat oven. LDH hydrothermal crystallization process was conducted for a desired time at 363 K. The capillary seals were detached after the hydrothermal process was completed, and the excess solution was removed by flushing the capillaries with N_2. What should be specially mentioned is such excess solution removed from capillary was collected and dried to get more powder of LDH films for further characterization. Thereafter, the capillary was flushed with DI water and dried overnight at 393 K. Finally, the capillary was calcined at 623 K for 6 h. By adjusting the concentration of the precursor solution and hydrothermal synthesis time, the morphology and thickness of the LDH film can be easily controlled.

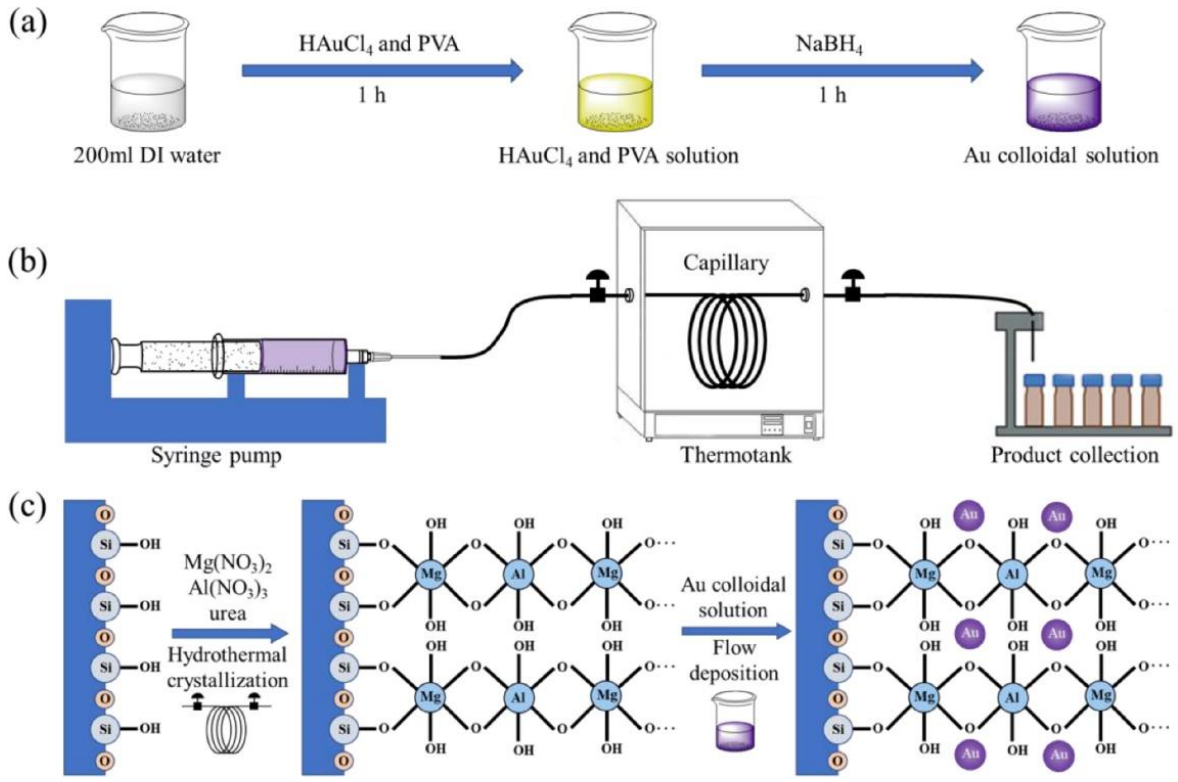

Fig. 1. (a) Preparation of Au colloidal solution. (b) Scheme of fabricating a Au/LDH film in a capillary microreactor. (c) Scheme of hydrothermal crystallization and the fixation of the Au nanoparticles inside the capillary microreactor.

For comparison, LDH powder catalyst was synthesized by a normal hydrothermal process. The LDH precursor solution with the same liquor composition as above was hydrothermally treated at 363 K for 72 h. After the reaction, the white solid was centrifuged, washed with DI water, and dried for 12 h at 393 K.

2.2.3. Immobilization of Au NPs in LDH film coated capillaries

Deposition-precipitation (DP) is the most well-known method for immobilization of metal nanoparticles on various substrate. However, DP method is not available for this experiment because of the corrosion of LDH film by gold chloride solution (Au 23.5–23.8 wt% in dilute HCl). For this reason, the immobilization of Au NPs on LDH film was performed by a flow deposition method. The flow deposition method was divided into two steps (Fig. 1a, b). In the first step, Au colloidal solution was prepared by using PVA as protecting agent [56]. In a typical preparation, 0.3 mL gold chloride solution was

dissolved in 200 mL DI water, followed by addition of 5 mL 0.3 wt% PVA aqueous solution (Fig. 1a). After stirring for 1.0 h under ambient conditions, 5 mL 0.1 mol/L $NaBH_4$ aqueous solution was quickly added. The color of the mixed solution turn from light yellow to purple black, which indicates the formation of Au colloidal solution. In the second step, the as-synthesized Au colloidal solution was injected into microchannel of LDH film coated capillary at a set flow rate of 20 μL/min for 1 h, 2 h and 3 h (Fig. 1b). Changing the flow time of Au colloidal solution through capillary can conveniently achieve the Au/LDH films with different Au loadings as 0.56 wt% for 1 h, 0.98 wt% for 2 h and 1.85 wt% for 3 h, respectively. Thereafter, the capillary was flushed with DI water and dried overnight at 393 K. Finally, the prepared capillary was calcined at 623 K for 6 h to achieve Au/LDH film capillary microreactors for further investigation (Fig. 1c).

For Au/LDH powder catalyst, 1 g as-synthesized MgAl-LDH powder was added in Au colloidal solution prepared by using PVA as protecting agent. After stirring overnight under the lightproof condition, the mixture turned to purplish black. After centrifugation, washed with DI water, and dried overnight at 393 K, the purple solid was collected. The calculated loading of Au on LDH powder is 1 wt%. Finally, the purple solid was calcined 623 K for 6 h to achieve Au/LDH powder catalyst for further investigation.

2.3. Characterization

X-ray diffraction (XRD) patterns of Au/LDH powder and dried thin film samples were recorded on a PANalytical X'Pert PRO powder diffractometer in step scan mode between 10° to 80° 2θ at a step of 0.0167° using Cu Kα radiation (λ= 0.1541 nm). Film thickness and morphology was collected on a HITACHI S-4700 field emission scanning electron microscope (FE-SEM) at an acceleration voltage of 15 kV after platinum coating. Elemental mapping of Au/LDH films was obtained with Gemini 500 coupled with energy dispersive X-ray spectroscopy (EDX). Au mean particle size of Au/LDH film and Au colloidal solution was all determined from the transmission electron microscope (TEM) image recorded on a Tecnai G2 F30 S-Twin transmission electron microscope. FTIR spectra were acquired using a Nicolet 6700 Fourier transform spectrometer. The XPS data of LDH powder and Au/LDH powder were recorded on a Kratos AXIS Ultra DLD, and the binding energies were calibrated using the C1s spectrum as the internal standard reference at 284.8 eV. The ICP-OES data were acquired by analyzing the mixture collected from outlet of capillary microreactor using Agilent 720ES.

2.4. Continuous-flow catalytic tests of glycerol carbonylation with urea

The continuous flow set-up for glycerol carbonylation with urea using Au/LDH film coated capillary microreactor was the same as Fig. 1b. The mixture of reactants, containing glycerol (0.5536 g), urea (0.3604 g) and DMSO (9 g) was continuously fed into capillary microreactor for the carbonylation reaction at 413 K. The modification of the flow rate of feeding allows to easily adjust the residence time of the reaction in the capillary microchannel. The feed flow rate was set as 10, 20, 30, 40, 50 and 60 μL/min, which corresponded to the residence times of 6.62, 3.31, 2.21, 1.65, 1.32 and 1.11 min, respectively. After the reactants were moved through the capillary microchannel, the product was collected from outlet and analyzed by gas chromatography. 0.2 mL of liquid product was transferred to a 5 mL microcentrifuge tubes with caps, then added silyl reagent (a mixture of 1 mL hexamethyldisilane, 0.025 mL trimethylchlorosilane and 1 mL N,N-dimethylformamide) and closed. A white NH_4Cl precipitate was formed after 30 min reaction under ambient conditions, then 0.2 mL of isopropylbenzene (10% in DMF) was added as an internal standard. With centrifugation at 3000 rpm for 3 min, the clear supernatant was analyzed by gas chromatography. The gas chromatography (Shimadzu, GC-2014) was equipped with a SE-54 column and a flame ionization detector. Conversion and selectivity values of the catalytic tests were calculated according to the following equation Eq. (1) and ((2)):

$$Conversion\ (\%) = \frac{\text{moles of glycerol converted}}{\text{moles of initial glycerol}} \times 100 \qquad (1)$$

$$\text{Selectivity to glycerol carbonate}\ (\%) = \frac{\text{moles of glycerol carbonate}}{\text{moles of converted glycerol}} \times 100 \qquad (2)$$

3. Results and discussion

3.1. Fabrication of Au/LDH film in capillary microreactor

Using a fused silica capillary as the microchannel substrate, Au/LDH thin films were fabricated inside. As shown in Fig. 2, the fabrication process included three steps: pretreatment of the fused silica capillary, *in situ* growth of the LDH film on the inner surface of the fused silica capillary and immobilization of active Au species on the LDH film. By adjusting the concentration and operation time of the precursor solution, the morphology and thickness of the LDH film and the loading amount of Au NPs could be easily optimized, thereby realizing a capillary microreactor. The method included three key points: 1) The inner wall of fused silica capillary was chemically modified by pretreatment process to form conductive surface properties for uniform growing of LDH crystals; 2) porous LDH film served both as catalyst and catalyst support for fixing Au species without agglomeration; 3) all processes including the fabrication of Au/LDH catalytic film inside capillary microchannel and the continuous-flow reaction of glycerol carbonylation with urea were facile and scalable.

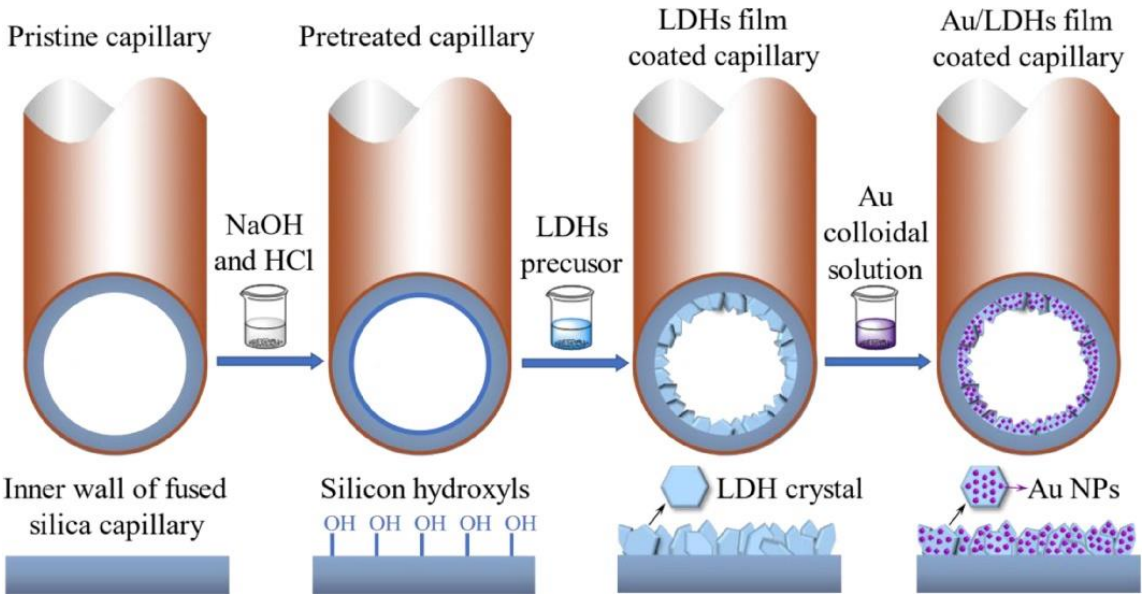

Fig. 2. Schematic illustration of the fabrication process for Au/LDH film coated capillary microreactor.

The inner wall of the pretreated fused silica capillary microchannel is uniform and smooth (Fig. 3a). The cross-sectional image in Fig. 3b also indicates that there is no obvious dissolution of the fused silica during the pretreatment. However, the silicon-oxygen bond cover the inner surface of the pristine capillary microchannel, providing little adhesion for the uniform growth of LDH crystallites. For this reason, the pretreatment was applied to activate the inner wall of the fused silica capillary by breaking silicon-oxygen bonds and producing silicon hydroxyls for enhancing surface activity and adsorption properties before film growth. After pretreatment, an uniform LDH film was formed on the inner surface of the pretreated capillary microchannel with a thickness of nearly 2 μm by homogeneous precipitation of LDH in hydrothermal crystallization process (Fig. 3c and d). The *ab*-faces of the *in situ* grown LDH crystallites perpendicular to the innerface of the capillary microreactors exhibited the high availability of the active basic sites exposed at the edges of the crystallites compared with the powdered form. Furthermore, the surface hydroxyl groups on the inner surface of capillary microchannel are favorable for the nucleation and growth of LDH film, which was consistent with previous studies [37]. XRD pattern (Fig. 3e) of the LDH powder obtained by drying the excess solution removed from the capillary showed all the characteristic peaks of LDH (PDF#35-1275), indicating that the obtained film on the inner surface of capillary microchannel exhibited the same crystal structure as the LDH powder. Furthermore, infrared spectroscopy was conducted to analyze the LDH film powder scraped off from the inner wall of capillary (Fig. 3f). The infrared spectrum of LDH film is consistent with that of LDH powder crystal. Therefore, the above results strongly proved that the film structure was indeed LDH crystal.

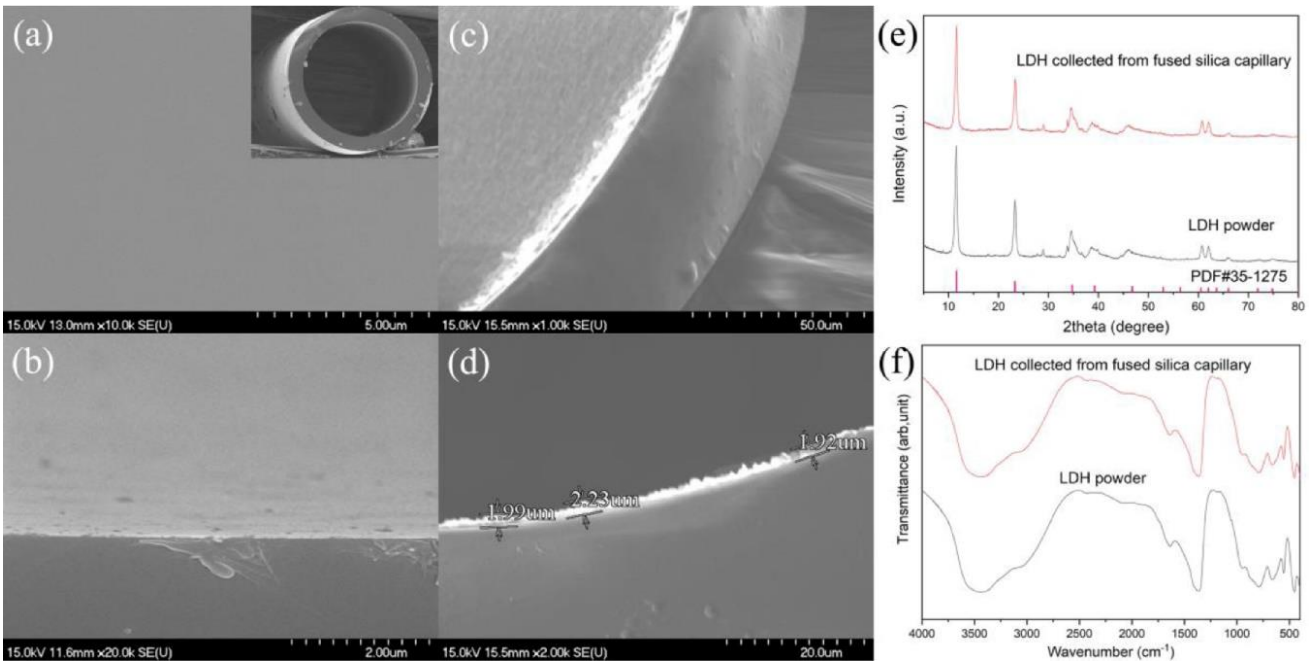

Fig. 3. (a) Top view image and (b) Cross-sectional image of pristine fused silica capillary inner surface (inset: pristine capillary). (c, d) SEM images of the LDH films in situ *grown on inner surface of capillary microchannel. (e) XRD pattern of MgAl-LDH samples. (f) FTIR spectra of LDH samples.*

3.2. Thickness of LDH film in capillary microreactor

It is noteworthy that the thickness of LDH film can be easily adjusted by changing the hydrothermal crystallization time. The potential relationship between hydrothermal crystallization time and the thickness of LDH film was explored by a cross-sectional study. The cross-section SEM images of the LDH film were shown in Fig. 4a-f, clearly depicted the growth of LDH crystallites with hexagonal plate-like morphology on the inner surface of capillary microchannels. LDH films exhibited different thicknesses (0.41, 0.6, 0.86, 1.18, 1.5 and 1.8 μm) under hydrothermal crystallization times of 12, 24, 36, 48, 60 and 72 h, respectively. Significantly, these findings indicated that there was a positive relationship between film thickness and hydrothermal crystallization time (Fig. S2). This relationship may be explained by the crystallization process of LDH crystals under urea hydrolysis. Firstly, the slowly hydrolysis of urea at 363 K in the capillary microchannels lead to the generation of hydroxide ions. $Al(OH)_3$ or AlO(OH) nucleate first and grow into small seed particles because of the lower solubility-product constant of Al^{3+} ions [57]. Then, these small seeds tend to aggregate together to minimize the overall energy of the system [58]. Sequentially, the initial MgAl-LDH crystal nuclei was formed by diffusion of Mg^{2+} ions from the mother solution to the matrix of $Al(OH)_3$ or AlO(OH) [57]. Finally, the MgAl-LDH crystals gradually grown up during hydrothermal synthesis time at these heterogeneous nucleation sites provided by the initial MgAl-LDH crystal nuclei. Previous studies reveal that hydrothermal synthesis time has a great influence on LDH crystallization [59]. Pseudo boehmite and aluminum hydroxide will be formed with no crystalline LDH phase if hydrothermal synthesis time less than 12 h [60]. As the extension of the hydrothermal synthesis time, MgAl-LDH crystals can be uniformly grown on the inner-wall of fused silica capillary and exhibit regular hexagonal platelet-like morphology with a thickness of about 100 nm. The height of these LDH crystallites with the *ab*-direction perpendicular to the inner surface of capillary microchannel ranges from 0.4 to 2 μm. In order to analyze the uniformity of the LDH film, the coated capillary under hydrothermal crystallization times of 72 h was divided in 3 sections of 10 cm length. The corresponding cross-sectional images at 10 cm (Fig. S3 a,b) and 20 cm (Fig. S3 c,d) of capillary showed that the LDH film was homogeneously coated along the inner wall of the capillary microreactor.

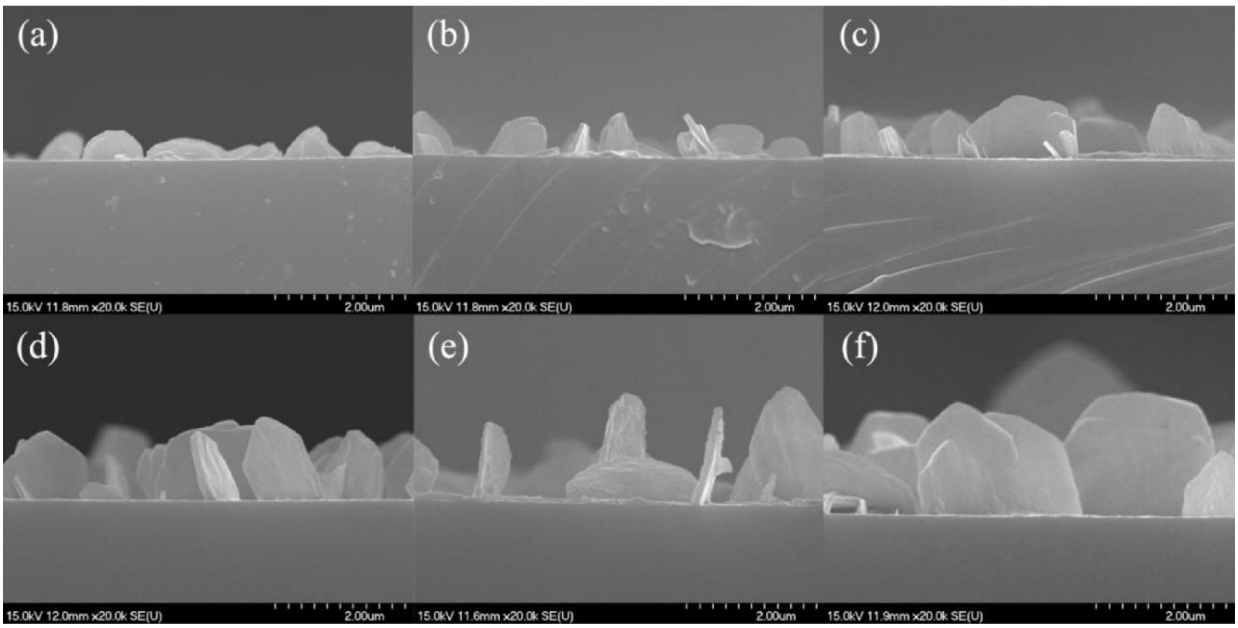

Fig. 4. SEM images of LDH films prepared on fused silica capillary wall at 363 K for different hydrothermal crystallization times: (a) 12 h, (b) 24 h, (c) 36 h, (d) 48 h, (e) 60 h and (f) 72 h.

3.3. Morphology of LDH film in capillary microreactor

Another important finding is that the morphology of as-synthesized LDH film inside capillary microchannel can be conveniently modulated by changing the concentration of LDH precursor solution. The previous study suggested that the LDH phase synthesized from urea hydrolysis exhibited mono-morphology of hexagonal platelet-like, and rosette-like morphology of LDH was achieved by hexamethylenetetramine hydrolysis with sodium stearate added [57]. However, the findings of the current study do not support the previous research. In this paper, tunable morphology of LDH film was achieved by altering the concentration of LDH precursor solution and slowly hydrolysis of urea at relatively low temperature (363 K). The top SEM patterns of LDH film in Fig. 5 revealed the morphological changes of LDH film at different concentrations of LDH precursor solution. In contrast to the blank capillary in Fig. 5a (inset: the cross section of capillary), the LDH film with sparse platelet-like morphology (Fig. 5b) was achieved at LDH precursor solution concentration of 0.04 mol/L (calculated by Mg^{2+}). As the concentration of LDH precursor solution increased, the crystal arrangement on the inner surface of capillary microchannel became more and more serried (Fig. 5c-d). This phenomenon might be explained by "evolutionary selection" [61]. The preferred orientation of LDH crystallites was often aligned with their *c*-axes essentially parallel to the substrate (*ab* face perpendicular to the substrate) [62]. When the concentration rises to 0.1 mol/L (calculated by Mg^{2+}), a hierarchical rosette-like microstructure appeared (Fig. 5e). This might be due to the growth of LDH crystallites with other orientations from the same nucleation site under higher LDH precursor solution concentration. Furthermore, the rosette-like LDH crystallites became denser during the concentration of the LDH precursor solution up to 0.2 mol/L (Fig. 5f). In order to exhibit a larger specific surface area for the adsorption of gold nanoparticles without affecting the flow state in the capillary microreactor, the LDH film with serried platelet-like morphology obtained at LDH precursor solution concentration of 0.067 mol/L (calculated by Mg^{2+}) was chosen as a typical LDH film for further investigation.

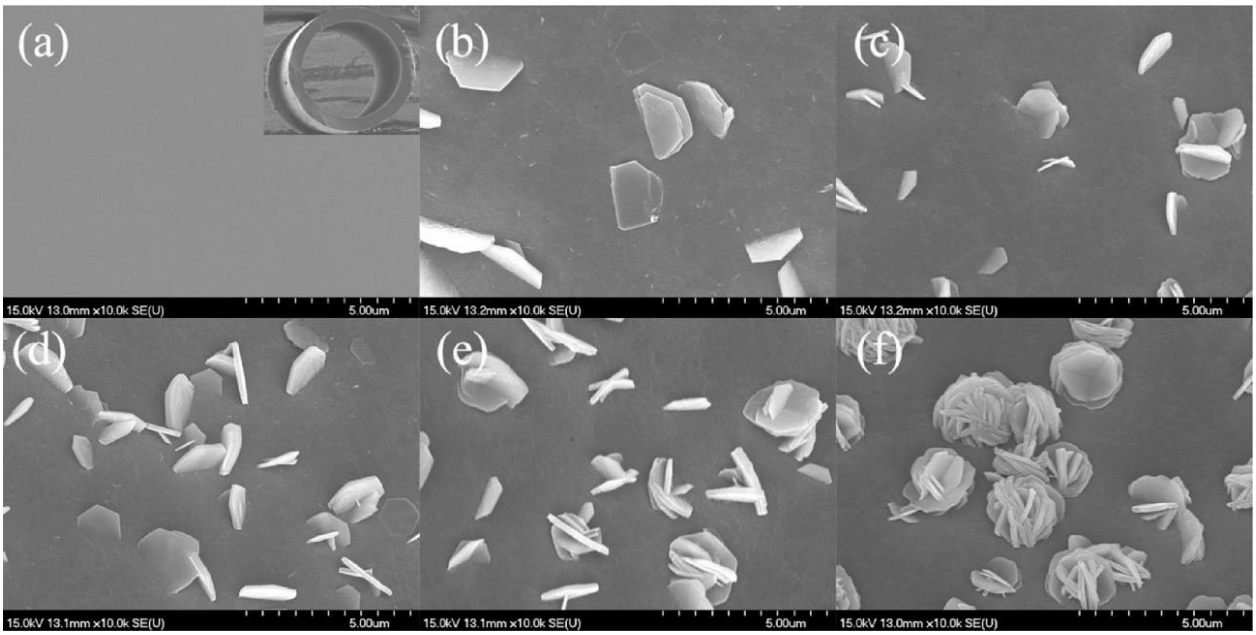

Fig. 5. SEM images of MgAl-LDH films synthesized from different concentrations of LDH precursor solution. (a) blank capillary, (b) 0.04 mol/L, (c) 0.05 mol/L, (d) 0.067 mol/L, (e) 0.1 mol/L, (f) 0.2 mol/L.

3.4. Immobilization of Au nanoparticles on LDH film in capillary microreactor

In the immobilization process, monodispersed Au nanoparticles were prepared and loaded on LDH film by flow deposition method to achieve a Au/LDH film coated capillary microreactor. Au colloidal solution was prepared by using PVA as protecting agent first. The as-prepared capillary microreactor with the LDH film thickness of approximately 1.8 μm was chosen as a model microchannel for immobilizing Au nanoparticles. Flow deposition method was utilized to deposit Au nanoparticles on LDH film in a capillary microreactor. Flow system could continuously provide a high concentration of Au colloid solution. Continuously flowing system ensured the high concentration of Au colloid solution moving through the capillary microchannel, and the loading amount of Au active component on LDH film can be manipulated by simply changing the flow time. In order to clearly illustrate the color change, the polyimide coating outside the fused silica capillary was removed after calcination at 773 K for 6 h. As shown in Fig. 6a, the pristine fused silica capillary was transparent, and the LDH film coated capillary microchannel became white. The color of the capillary microchannel gradually turned from white to light purple after loading Au NPs on the LDH film. TEM analysis revealed that the as-synthesized Au colloidal nanoparticles are almost monodispersed (Fig. 6b), and the mean diameter (number weighted average) for a typical Au particle size was 1.7 ± 0.5 nm (Fig. S4). However, when Au nanoparticles were immobilized on LDH film (Fig. 6c), the average particle size remained around 2 nm with a little increase after calcination (Fig. S5). For comparison, micrographs of Au colloidal nanoparticles were deposited on dried LDH powder and were recorded (Fig. S6). The average particle size and particle size distribution of Au nanoparticles immobilized inside LDH film coated microchannel (2.3 ± 0.5 nm) or on dried LDH powder support (2.5 ± 0.6 nm) are in agreement (Fig. S7). XRD pattern (Fig. 6d) of the Au/LDH film powder collected from the film counterpart shows the characteristic peaks of calcined LDH and Au (PDF#04-0784), indicating that the crystals of the LDH film are well preserved during the deposition of Au colloidal nanoparticles. Furthermore, elemental analysis of the Au/LDH film was conducted by EDX. An overlay of magnesium, aluminum and Au EDX maps is shown in Fig. 6f, g and h, which are relevant to the cross-sectional image in Fig. 6e, indicating a clear separation of the three elements and confirming the high dispersion of Au species in LDH film.

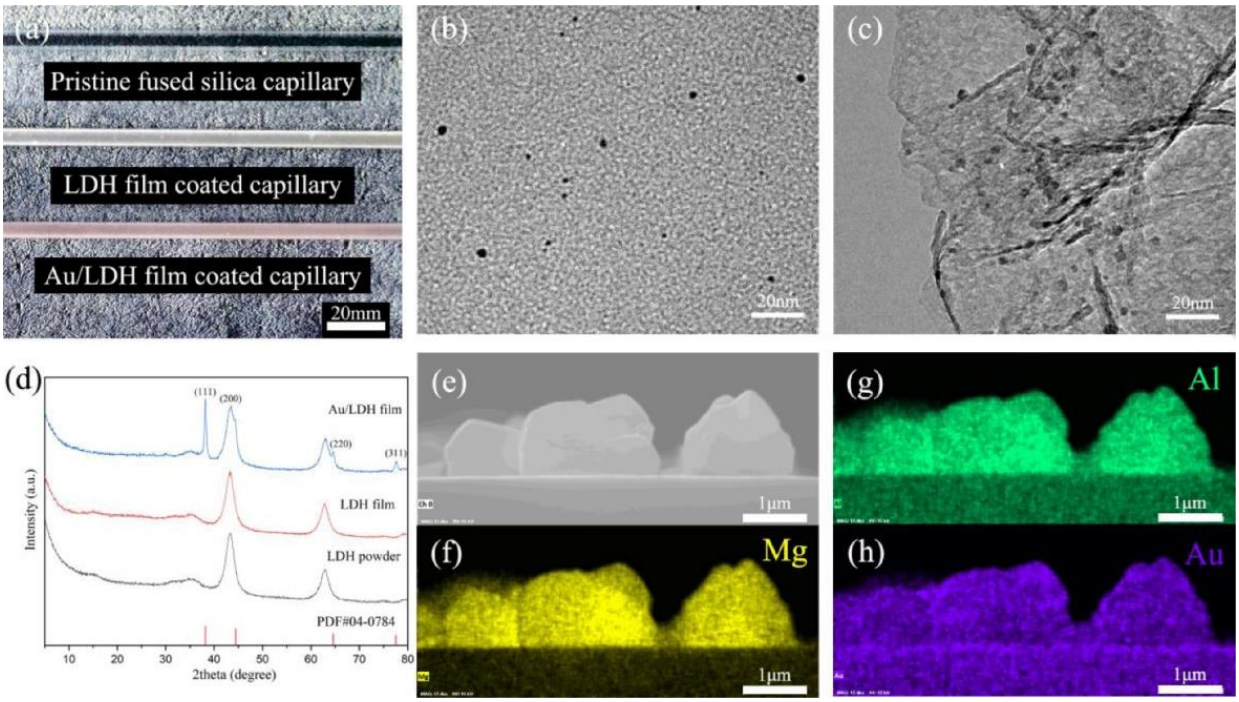

Fig. 6. Characterization of Au/LDH film coated capillary microchannel. (a) The images of different fused silica capillaries. (b) TEM data for Au nanoparticles suspended in water. (c) Typical TEM micrograph and (d) XRD patterns of the Au/LDH film. (e) SEM images of Au/LDH film and (f, g, h) the corresponding element maps.

3.5. Catalytic performance of Au/LDH film in capillary microreactor

For the traditional synthesized process of glycerol carbonylation with urea, the continuous generation of ammonia and its accumulation near the active site of catalyst hindered the forward reaction. The breaking of carbon bonds in glycerol under reduced pressure and hydroxyl groups in glycerol combined to form ether bonds and water also lead to a low productivity of GLC. The application of the Au/LDH film capillary microreactor removed ammonia from the vicinity of the active site in real time to ensure the stability of the forward reaction rate, and improved the productivity of GLC under mild conditions. The as-synthesized Au/LDH powder catalyst had the same Au loading as 0.98%/LDH film catalyst reached approximately 1 wt%. The contrast experiment was applied to investigate their catalytic performance of glycerol carbonylation with urea. Fig. 7a depicted the comparison of catalytic performance of powder catalysts (1 wt% Au loading) in batch reactor and catalytic film (0.98% Au/LDH film) in continuous flow capillary microreactor. The LDH film in capillary microreactor exhibited better catalytic performance than LDH powder catalyst. This might be the result of the enhanced mass transfer in the microchannel [63], which further illustrated that the LDH film not only served as a support of Au nanoparticles but also had a synergistic catalytic effect along with Au. Moreover, the loading of Au species improved the productivity of GLC in catalyst types of either powder or film, which was consistent with the previous study [64]. The Au/LDH film in the capillary microreactor showed the best GLC yield of 31.9% and highest GLC productivity of 3.78 $g \cdot h^{-1} \cdot g^{-1}$. Subsequently, the reaction conditions were further optimized for catalytic film of Au/LDH. Contrastive reactions were performed by varying the molar ratios of glycerol to urea from 0.5 to 4 at 413 K (Fig. 7b). When the molar ratio of glycerol to urea was 1, the best catalytic performance was observed and also consistent with previously reported results [52]. With further increase of glycerol, GLC productivity gradually decreased because of insufficient amount of urea. Hence, the optimum molar ratio of glycerol to urea was selected at 1:1 for further research. The typical curve in Fig. 7c illustrated the influence of reaction temperature on carbonylation reaction. The yield and productivity of GLC apparently increased with the rise of reaction temperature firstly and then decreased with further heating. This phenomenon might be contributed to the fact that higher reaction temperature significantly reduced the GLC productivity by aggravating undesired reactions. Thereby, the optimum reaction temperature in the capillary microreactor for glycerol carbonylation with urea was 413 K.

It was common knowledge that flow rate had a great influence on the catalytic performance in capillary microreactor functionalized with catalytic film. Three capillary microreactors with various Au species had been fabricated by changing the flow deposition time (1h, 2h and 3h) for immobilizing Au NPs. The Au loading of three Au/LDH films reached 0.56 wt%, 0.98 wt% and 1.85 wt% (calculated from EDX results in Fig. S8) under different flow deposition time, respectively.

Such three capillary microreactors were utilized for glycerol carbonylation with urea under the typical reaction condition mentioned above. As shown in Fig. 7d, the GLC productivity of the three capillary microreactors were close to 1.2 $g \cdot h^{-1} \cdot g^{-1}$ at the reactants flow rate of 10 μL/min. The residence time was inversely proportional to the flow rate, the GLC yield gradually decreased while the GLC productivity showed a trend of increase before decrease with the further increase of flow rate thereby. Therefore, the rising of flow rate signified the decrease of the residence time, resulting in less contact time of the reactants with active components and GLC yield declined thereby. Compared with the sharp decrease in 0.56 wt% Au/LDH and 0.98 wt%Au/LDH microreactor, the yield of 1.85 wt% Au/LDH in the flow range of 10-20 μL/min achieved 31.9%. The yield of GLC in 1.85%Au/LDH microreactor decreased to 25% at the flow range of 40 μL/min while the productivity rised to 3.15 $g \cdot h^{-1} \cdot g^{-1}$, and the productivity finally stabilized at 2.57 $g \cdot h^{-1} \cdot g^{-1}$ at flow range of 60 μL/min. Interestingly, 0.98% Au/LDH microreactor exhibited higher productivity to 2.88 $g \cdot h^{-1} \cdot g^{-1}$ than 2.35 and 2.57 $g \cdot h^{-1} \cdot g^{-1}$ in 0.56 wt%Au/LDH and 1.85 wt%Au/LDH microreactor at flow range of 60 μL/min, respectively. This indicated that the 0.98 wt%Au/LDH film coated capillary microreactor involved sufficient loading of Au NPs for the reaction and exhibited better catalytic properties at high flow range under the same conditions.

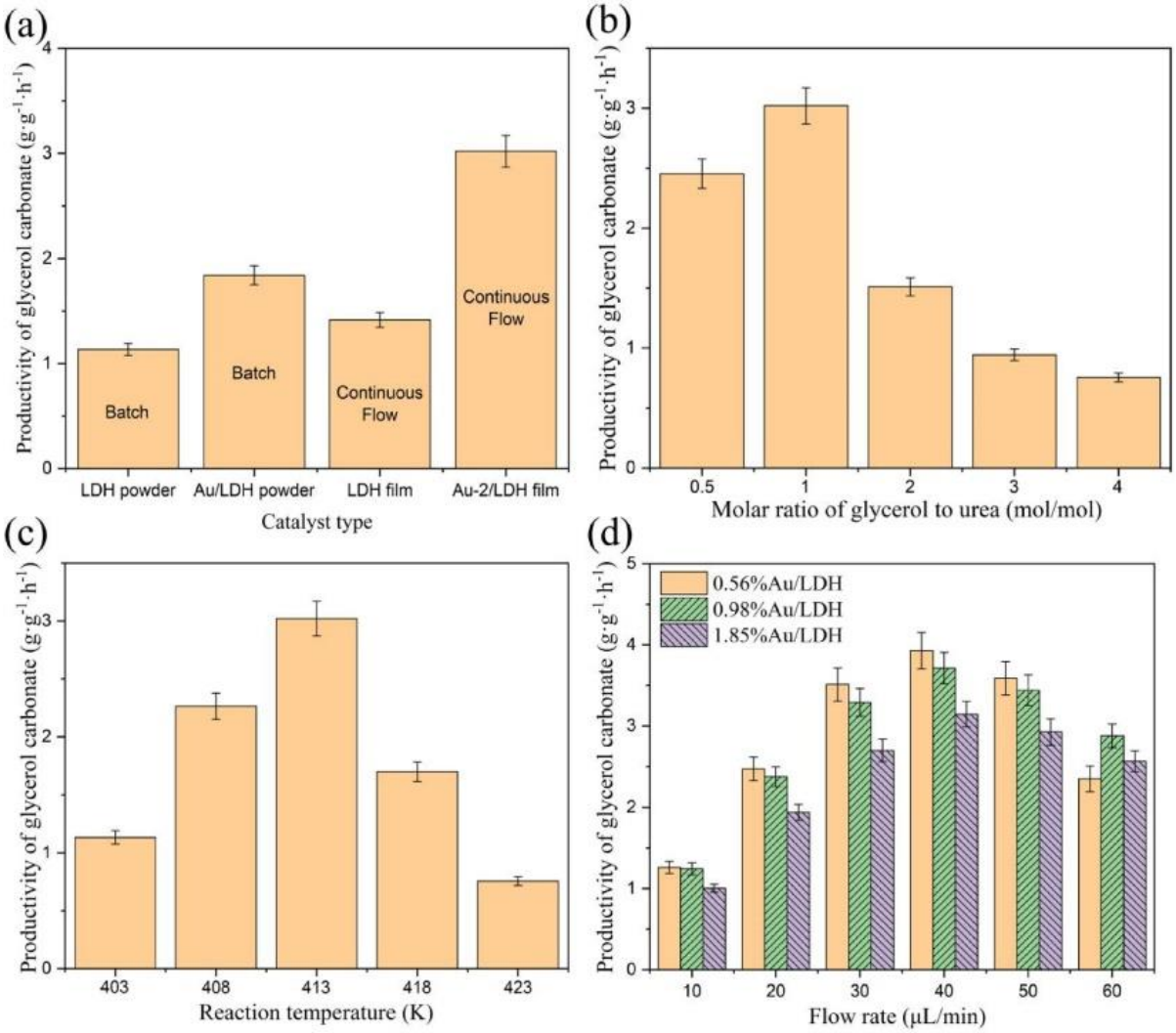

Fig. 7. Influence of reaction conditions on glycerol carbonylation with urea. (a) Influence of catalyst types. Reaction conditions: T=413 K; flow rate = 20 μL/min; $n_{glycerol}/n_{urea}$ = 1; reaction time for batch reaction = 1 h. (b) Influence of molar ratio of glycerol to urea. Reaction conditions: T=413 K; flow rate = 20 μL/min; catalyst coating: 0.98%Au/LDH. (c) Influence of reaction temperature. Reaction conditions: flow rate = 20 μL/min; $n_{glycerol}/n_{urea}$ = 1; catalyst coating: 0.98%Au/LDH. (d) Influence of flow rate. Reaction conditions: T=413 K; $n_{glycerol}/n_{urea}$ = 1.

3.6. Stability of Au/LDH film in capillary microreactor

In general, the industrial application of capillary microreactors often required long-term stability. The stable catalytic performance of 0.98 wt%Au/LDH capillary microreactor was conducted at reactants flow rate of 20 μL/min to study the stability of the microreactor. A detailed life time study of 0.98 wt%Au/LDH capillary microreactor had been performed for 30 h, during which products were collected every 2 h. No obvious decrease of catalytic performance in 0.98 wt%Au/LDH capillary microreactor was observed, the yield and productivity of GLC remained at nearly 31.9% and 2.38 $g \cdot h^{-1} \cdot g^{-1}$ throughout the reaction (Fig. 8a). This implied that the as-prepared capillary microreactor was rather stable for catalytic carbonylation of glycerol and urea. The cross-sectional SEM image of Au/LDH film after reaction indicated that no peeling off or damage was observed in 30h on stream (Fig. 8b). The uniform dispersion of Au NPs in the LDH film was confirmed by EDX mapping analysis of spent Au/LDH film (Fig. 8c-d). Furthermore, XPS spectra were employed to investigate the chemical states and surface elemental compositions of Au/LDH powder catalysts. Core-levels like Mg 1s, Mg 2p, Al 2s, Al 2p, O 1s, Au 4f and C 1s can be identified in the full survey spectra for 1% Au/LDH powder (Fig. S9 and Fig. S10).

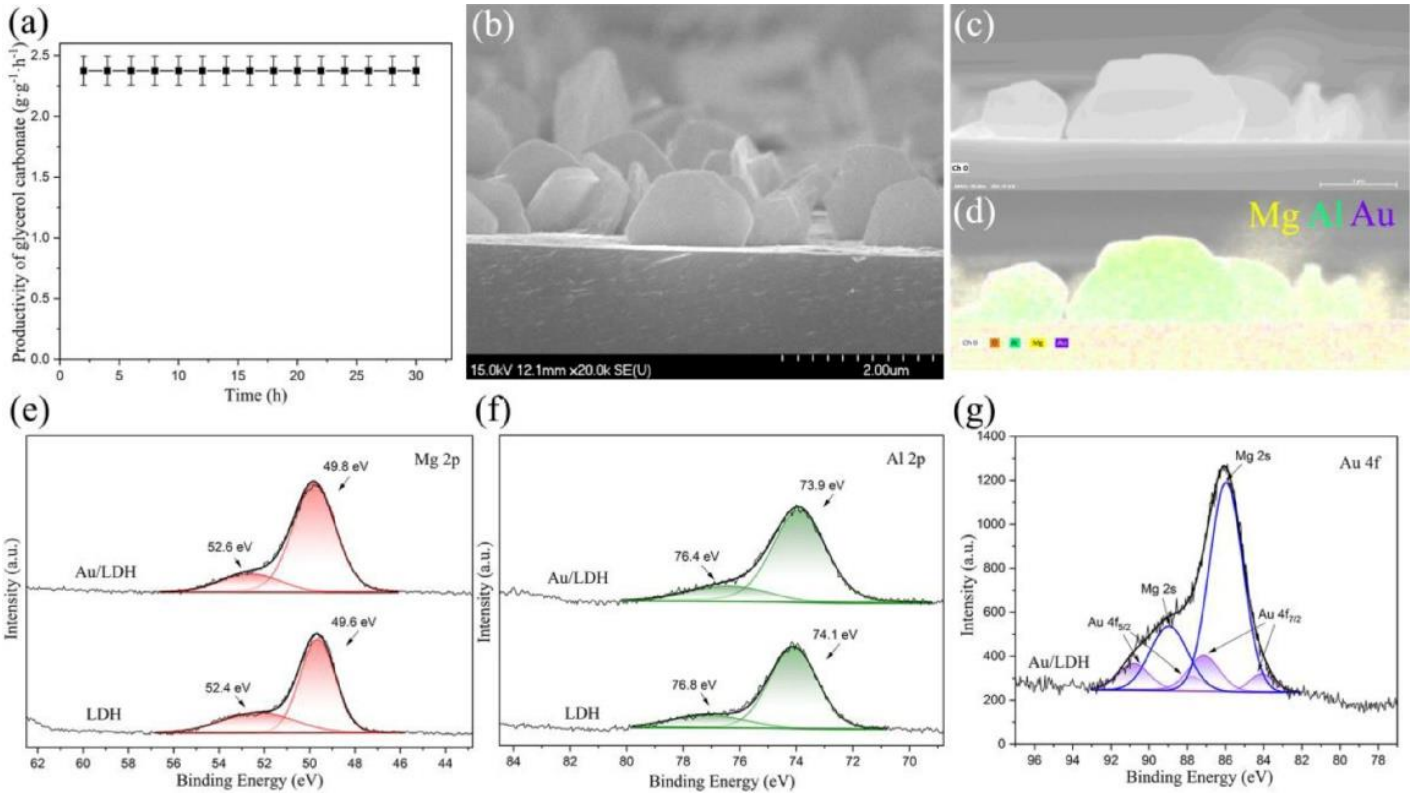

Fig. 8. (a) Catalytic properties of long-term run in Au-3/LDH film capillary microreactor for 30 h at the reactants flow rate of 20 μL/min). (b) Cross-sectional SEM image and (c, d) EDX mapping analysis of the 0.98%Au/LDH film structure after reaction. (e-g) XPS survey spectra for Au/LDH powder, and high-resolution XPS spectra of Mg 2p (e), Al 2p (f) and Au 4f (g).

Mg 2p XPS spectra of pristine LDH powder and 1 wt%Au/LDH powder could be fitted with two doublets (Fig. 8d). The first peak at binding energies of 49.6 eV for LDH and 49.8 eV for Au/LDH, were associated with Mg^{2+} atoms in LDH sturcture. The second peak at binding energies of 52.4 eV for LDH and 52.6 eV for 1 wt%Au/LDH corresponded to Mg atoms in strong interaction with Al atoms in the mixed oxide producing Mg-O-Al bonds [65]. The Al 2p XPS spectra for pristine LDH powder and 1 wt%Au/LDH powder were shown in Fig. 8e. The two main peaks appearing at 73.9 and 74.1 eV were assigned to Al^{3+} in octahedral coordination that returned to the LDH structure. Another two weak peaks centered at 76.4 and 76.8 eV were attributed to those octahedrally coordinated in the alumina phase or those in strong interaction with Mg atoms forming Mg-O-Al bonds.

The XPS spectra of Au 4f obtained from 1 wt%Au/LDH was showed in Fig. 8f. Deconvoluted Au 4f spectra of 1 wt%Au/LDH powder showed peaks corresponding to two states of Au. The peaks of 1 wt%Au/LDH centered at 84.1 and 87.8 eV could be assigned to Au^0, and the peaks located at the binding energy of 87.1 and 90.8 eV were corresponding to $Au(III)Cl_4^-$ ions [66]. In addition, the peaks located at the binding energy of 87.1 eV was the overlap of $4f_{7/2}$ for $Au(III)Cl_4^-$

and $4f_{5/2}$ for the Au^0. The strong peak centered at 89 eV was associated with the overlap of the Mg 2s and Au 4f. The peaks of $Au(III)Cl_4^-$ ions in 1 wt%Au/LDH revealed that the $Au(III)Cl_4^-$ anions were difficult to be reduced as the protection of the inter gallery. This also indicated the incorporation of $Au(III)Cl_4^-$ anions into the interlayer, but not simple adsorption on the surface of LDH, which in accordance with the abovementioned XRD, SEM and TEM results. Moreover, due to the coexistence of Au metallic state and $Au(III)Cl_4^-$ anions, 1 wt%Au/LDH powder catalyst exhibited lower productivity of GLC than other supported Au catalyst in previous studies [51,64].

3.7. Au leaching in Au/LDH film capillary microreactor

Leaching of the active metal into the liquid phase was also important in the design of inner wall coated capillary microreactors. Metal leaching due to the flow of reactants through the capillary was analyzed by Inductively Coupled Plasma Optical Emission Spectrometer (ICP-OES). The liquid effluent from the microreactor was collected to test the leaching of Au. The results summarized in Table S1 showed that the capillary microreactor with 0.56 wt%Au/LDH film, 0.98 wt%Au/LDH film and 1.85 wt%Au/LDH film coated showed 3.7%, 4.2% and 4.5% of Au leaching during the stability tests, respectively. It agreed with previous report that higher catalyst loading might lead to the higher leaching of catalysts [67]. Nevertheless, the loss in Au content did not cause obvious decline in productivity (Fig. 8a). This indicated that metal active sites was not decreased during the loss of Au content. On this basis, it was concluded that Au leaching had little impact on catalytic performance of Au/LDH film during continuous flow catalytic carbonylation of glycerol over 30 h time-on-stream.

3.8. Comparison of Au/LDH film in capillary microreactor with other reported representative solid catalyst

Catalytic performance of Au/LDH film in capillary microreactor was compared with other solid catalysts reported previously (Table 1). Obviously, pristine MgO showed much lower activity than other mixed oxide powder catalysts [64] mainly due to the presence of only strong basic sites on their surface. Although Au supported catalysts had high GLC productivity, the catalyst cost in product separation process was also very high [51, 64]_ENREF_49. While the GLC productivity of the bulk MgAl mixed oxide was clearly superior [52], it was important to remind that the capillary microreactor in present work only contains a thin LDH film immobilized by Au NPs. The moderate yield and productivity of GLC (31.9% and 3.78 $g{\cdot}h^{-1}{\cdot}g^{-1}$) was achieved in such capillary microreactor from carbonylation of glycerol with urea under atmospheric pressure without any purge gas. Furthermore, the preparation process of this capillary microreactor was simple and easy to scale up.

Table 1
Comparison of catalytic activity of Au/LDH film in capillary microreactor with other reported solid catalysts.

Catalyst	Reactor type	Reaction temperature (K)	Reaction time (h)	Reaction pressure (kPa)	Purge gas flow	Glycerol carbonate productivity ($g{\cdot}h^{-1}{\cdot}g^{-1}$)[a]	Reference
MgO[b]	batch	423	4	AP[c]	N_2	4.60	[64]
Au/MgO[b]	batch	423	4	AP[c]	N_2	9.91	[64]
AuPd/MgO[b]	batch	383	4	AP[c]	N_2	11.86	[51]
Mg/Al/Zr hydrotalcite	batch	413	3	10	None	8.63	[68]
Mg/Al mixd oxide[d]	Continuous flow	423	-	1	None	5.48[e]	[52]
Au/LDH film	Continuous flow	413	-	AP[c]	None	3.78[f]	Present work

[a] Productivity: (g of product per h per g of catalyst).
[b] Reaction conditions: glycerol/urea molar ratio: 1: 1.5, catalyst: 0.25 g.
[c] AP: Atmospheric Pressure.
[d] Reaction conditions: glycerol/urea molar ratio: 1: 1, catalyst: 0.5 g, particle size = 0.2-0.4 mm.
[e] Reaction conditions: 0.006 mol glycerol and 0.006 mol urea, 0.1 g of catalyst and 9 g of solvent, flow rate = 100 μL/min;
[f] Reaction conditions: 0.006 mol glycerol and 0.006 mol urea, 0.01 g of catalyst and 7 ml of solvent, flow rate = 20 μL/min.

The above results indicated that as-prepared capillary microreactor was an efficient, and stable microchannel reactor, which had great potential in practical applications.

4. Conclusions

A simple and facile method was developed to fabricate an active Au/LDH film-coated capillary microreactor for catalytic carbonylation of glycerol with urea. This strategy was based on both *in situ* hydrothermal growth of LDH film on the inner wall after enhancing surface activity and adsorption properties by pretreatment and loading of Au nanoparticles onto surface of LDH crystals by flow deposition process, leading to a continuous and uniform Au/LDH film as well as evenly dispersed and stably fixed Au nanoparticles on the film. Through adjusting the concentration of the LDH precursor solution,

hydrothermal synthesis time and flow deposition time, various Au/LDH films with thickness from 0.41 to 1.8 mm, morphology from platelet-like to rosette-like and Au loading from 0.56 wt% to 1.98 wt% could be established in capillary microchannel. The yield of glycerol carbonate reached 31.9% at flow rate of 10 μl/min and reaction temperature of 413 K under atmospheric pressure. The maximum productivity of 3.78 $g \cdot h^{-1} \cdot g^{-1}$ was obtained at flow rate of 40 μl/min under same reaction temperature and pressure. The 0.98 wt%Au/LDH film capillary microreactor also retained a productivity of 2.38 $g \cdot h^{-1} \cdot g^{-1}$ for glycerol carbonylation with urea over a time scale of 30 h, indicating good stability and catalytic activity, which could be attributed to the synergetic contribution from LDH film and Au NPs inside the capillary microchannel. This work provided a route for fabricating other diatomic and triatomic metal LDH films immobilizing metal nanoparticles inside microchannel for other heterogeneous catalytic systems.

CRediT authorship contribution statement

Qi Ming She: Conceptualization, Investigation, Writing – original draft, Writing – review & editing. **Jia Hui Liu:** Methodology, Investigation, Data curation. **Cyril Aymonier:** Writing – review & editing. **Chun Hui Zhou:** Conceptualization, Supervision, Writing – review & editing, Project administration, Funding acquisition.

Declaration of Competing Interest

All authors have read and approved its content and 'No Conflict' of interest by all authors exist in the submission of this manuscript.

Acknowledgement

This research was financially supported by the National Natural Science Foundation of China (22072136, 41701334), the funding from The State Key Laboratory Breeding Base of Green Chemistry-Synthesis Technology, The Zhejiang University of Technology (GCTKF2014006), from Engineering Research Center of Non-metallic Minerals of Zhejiang Province, Zhejiang Institute of Geology and Mineral Resource, China (ZD2020K07), from the Research Foundation of Education Bureau of Anhui Province, China (KJHS2016B09).

Appendix. Supplementary materials

References

1. A. Renken, L. Kiwi-Minsker. **Chapter 2 - Microstructured catalytic reactors,** *in :* B.C. Gates, H. Knözinger (Eds.), Advances in Catalysis, Academic Press (2010), pp. 47-122.
2. J. Zhang, K. Wang, A.R. Teixeira, K.F. Jensen, G. Luo. Annu. Rev. Chem. Biomol. Eng., 8 (2017), pp. 285-305.
3. A. Tanimu, S. Jaenicke, K. Alhooshani. Chem. Eng. J., 327 (2017), pp. 792-821.
4. P.L. Suryawanshi, S.P. Gumfekar, B.A. Bhanvase, S.H. Sonawane, M.S. Pimplapure. Chem. Eng. Sci., 189 (2018), pp. 431-448.
5. V. Paunovic, V. Ordomsky, M.F. Neira D'Angelo, J.C. Schouten, T.A. Nijhuis. Ind Eng. Chem. Res., 54 (2015), pp. 2919-2929.
6. V. Paunovic, V. Ordomsky, M. Fernanda Neira D'Angelo, J.C. Schouten, T.A. Nijhuis. J. Catal., 309 (2014), pp. 325-332.
7. S. Kanungo, V. Paunovic, J.C. Schouten, M.F. Neira D'Angelo. Nano Lett., 17 (2017), pp. 6481-6486.
8. A.J. Exposito, Y. Bai, K. Tchabanenko, E.V. Rebrov, N. Cherkasov. Ind. Eng. Chem. Res., 58 (2019), pp. 4433-4442.
9. E.V. Rebrov, A. Berenguer-Murcia, H.E. Skelton, B.F.G. Johnson, A.E.H. Wheatley, J.C. Schouten. Lab Chip, 9 (2009), pp. 503-506.
10. Z. He, Y. Li, Q. Zhang, H. Wang. Appl. Catal. B, 93 (2010), pp. 376-382.
11. L. Zhang, Z. Liu, Y. Wang, R. Xie, X.-J. Ju, W. Wang, L.-G. Lin, L.-Y. Chu. Chem. Eng. J., 309 (2017), pp. 691-699.

12. L.A. Truter, P.R. Makgwane, B. Zeelie, S. Roberts, W. Böhringer, J.C.Q. Fletcher. Chem. Eng. J., 257 (2014), pp. 148-158.
13. G. Zhang, L. Zhang, X. Wang, A. Chen, Q. Zhang. React. Chem. Eng., 5 (2020), pp. 539-546.
14. X. Huang, G. Zhang, L. Zhang, Q. Zhang. ACS Omega,, 5 (2020), pp. 20784-20791.
15. Y. Liu, N. Wang, J.H. Pan, F. Steinbach, J. Caro. J. Am. Chem. Soc., 136 (2014), pp. 14353-14356.
16. W. Li, R. Sreerangappa, J. Estager, J.-C.M. Monbaliu, D.P. Debecker, P. Luis. Chem. Eng. Process., 132 (2018), pp. 127-136.
17. T. Inoue, J. Adachi, K. Ohtaki, M. Lu, S. Murakami, X. Sun, D.F. Wang. Chem. Eng. J., 278 (2015), pp. 517-526.
18. D. van Herk, P. Castaño, M. Makkee, J.A. Moulijn, M.T. Kreutzer. Appl. Catal. A, 365 (2009), pp. 199-206.
19. R.L. Papurello, J.L. Fernández, E.E. Miró, J.M. Zamaro. Chem. Eng. J., 313 (2017), pp. 1468-1476.
20. A. Karim, J. Bravo, D. Gorm, T. Conant, A. Datye. Catal. Today, 110 (2005), pp. 86-91.
21. J. Yu, Q. Wang, D. O'Hare, L. Sun. Chem. Soc. Rev., 46 (2017), pp. 5950-5974.
22. O. Pascu, S. Marre, B. Cacciuttolo, G. Ali, L. Hecquet, M. Pucheault, V. Prevot, C. Aymonier. ChemNanoMat, 3 (2017), pp. 614-619.
23. Q. Wang, D. O'Hare. Chem. Rev., 112 (2012), pp. 4124-4155.
24. H.R. Prakruthi, B.M. Chandrashekara, B.S. Jai Prakash, Y.S. Bhat. Catal. Sci. Technol., 5 (2015), pp. 3667-3674.
25. H.R. Prakruthi, B.S. Jai Prakash, Y.S. Bhat. J. Mol. Catal. A, 408 (2015), pp. 214-220.
26. I. Cota, E. Ramírez, F. Medina, G. Layrac, D. Tichit, C. Gérardin. J. Mol. Catal. A, 412 (2016), pp. 101-106.
27. B. Ma, A. Fernandez-Martinez, S. Grangeon, C. Tournassat, N. Findling, S. Carrero, D. Tisserand, S. Bureau, E. Elkaïm, C. Marini, G. Aquilanti, A. Koishi, N.C.M. Marty, L. Charlet. Environ. Sci. Technol., 52 (2018), pp. 1624-1632.
28. M. Morikawa, N. Ahmed, Y. Yoshida, Y. Izumi. Appl. Catal. B, 144 (2014), pp. 561-569.
29. A. Chatterjee, P. Bharadiya, D. Hansora. Appl. Clay Sci., 177 (2019), pp. 19-36.
30. X. Zou, A. Goswami, T. Asefa. J. Am. Chem. Soc., 135 (2013), pp. 17242-17245.
31. L. Li, L. Dou, H. Zhang. Nanoscale, 6 (2014), pp. 3753-3763.
32. S. Li, C.I. Ezugwu, S. Zhang, Y. Xiong, S. Liu. Appl. Surf. Sci., 487 (2019), pp. 260-271.
33. K. Iqbal, A. Iqbal, A.M. Kirillov, B. Wang, W. Liu, Y. Tang. J. Mater. Chem. A, 5 (2017), pp. 6716-6724.
34. N. Arora, A. Mehta, A. Mishra, S. Basu. Appl. Clay Sci., 151 (2018), pp. 1-9.
35. Z. Lü, F. Zhang, X. Lei, L. Yang, S. Xu, X. Duan. Chem. Eng. Sci., 63 (2008), pp. 4055-4062.
36. Y. Dou, S. Xu, X. Liu, J. Han, H. Yan, M. Wei, D.G. Evans, X. Duan. Adv. Funct. Mater., 24 (2014), pp. 514-521.
37. X. Guo, F. Zhang, D.G. Evans, X. Duan. Chem. Commun. (Camb.), 46 (2010), pp. 5197-5210.
38. M. Shao, F. Ning, J. Zhao, M. Wei, D.G. Evans, X. Duan. Adv. Funct. Mater., 23 (2013), pp. 3513-3518.
39. Y. Zhang, P. Yu, J. Wang, Y. Li, F. Chen, K. Wei, Y. Zuo. Appl. Surf. Sci., 433 (2018), pp. 927-933.
40. J. Zhao, J. Chen, S. Xu, M. Shao, Q. Zhang, F. Wei, J. Ma, M. Wei, D.G. Evans, X. Duan. Adv. Funct. Mater., 24 (2014), pp. 2938-2946.
41. S. Li, S. Mo, D. Wang, X. Wu, Y. Chen. Catal. Today, 332 (2019), pp. 132-138.
42. I. Reyero, I. Velasco, O. Sanz, M. Montes, G. Arzamendi, L.M. Gandía. Catal. Today, 216 (2013), pp. 211-219.
43. W. Xu, L. Gao, G. Xiao. Fuel, 159 (2015), pp. 484-490.
44. F.Javier Echave, O. Sanz, L.C. Almeida, J.A. Odriozola, M. Montes. **Highly porous hydrotalcite-like film growth on anodised aluminium monoliths,** *in:* E.M. Gaigneaux, M. Devillers, S. Hermans, P.A. Jacobs, J.A. Martens, P. Ruiz (Eds.), Studies in Surface Science and Catalysis, Elsevier (2010), pp. 639-642.

45. K. Kong, D. Li, W. Ma, Q. Zhou, G. Tang, Z. Hou. Chin. J. Catal., 40 (2019), pp. 534-542.

46. N. Lei, Z. Miao, F. Liu, H. Wang, X. Pan, A. Wang, T. Zhang. Chin. J. Catal., 41 (2020), pp. 1261-1267.

47. G.M. Lari, G. Pastore, M. Haus, Y. Ding, S. Papadokonstantakis, C. Mondelli, J. Pérez-Ramírez. Energy Environ. Sci., 11 (2018), pp. 1012-1029.

48. E. Elhaj, H. Wang, Y. Gu. Mol. Catal., 468 (2019), pp. 19-28.

49. M. Marimuthu, P. Marimuthu, S.K A.K., S. Palanivelu, V. Rajagopalan. Mol. Catal., 460 (2018), pp. 53-62.

50. S. Arora, V. Gosu, V. Subbaramaiah. Mol. Catal., 496 (2020), Article 111188.

51. M. Hasbi Ab Rahim, Q. He, J.A. Lopez-Sanchez, C. Hammond, N. Dimitratos, M. Sankar, A.F. Carley, C.J. Kiely, D.W. Knight, G.J. Hutchings. Catal. Sci. Technol., 2 (2012), pp. 1914-1924.

52. G.M. Lari, A.B.L. de Moura, L. Weimann, S. Mitchell, C. Mondelli, J. Pérez-Ramírez. J. Mater. Chem. A, 5 (2017), pp. 16200-16211.

53. H. Nguyen-Phu, L.T. Do, E.W. Shin. Catal. Today, 352 (2020), pp. 80-87.

54. D.M. Chaves, M.J. Da Silva. New J. Chem., 43 (2019), pp. 3698-3706.

55. F. Zhang, X.-H. Wu, M. Yao, Z. Fang, Y.-T. Wang. Green Chem., 18 (2016), pp. 3302-3314.

56. M. Comotti, W.-C. Li, B. Spliethoff, F. Schüth. J. Am. Chem. Soc., 128 (2006), pp. 917-924.

57. J. Yu, G. Fan, Y. Yang, F. Li. J. Colloid Interface Sci., 432 (2014), pp. 1-9.

58. S. Mo, S. Li, J. Li, Y. Deng, S. Peng, J. Chen, Y. Chen. Nanoscale, 8 (2016), pp. 15763-15773.

59. M. Ogawa, H. Kaiho. Langmuir, 18 (2002), pp. 4240-4242.

60. M. Adachi-Pagano, C. Forano, J.-P. Besse. J. Mater. Chem., 13 (2003), pp. 1988-1993.

61. F.-Z. Zhang, M. Fuji, M. Takahashi. Chem. Mater., 17 (2005), pp. 1167-1173.

62. X. Guo, F. Zhang, S. Xu, D.G. Evans, X. Duan. Chem. Commun. (Camb.) (2009), pp. 6836-6838.

63. K. Sai Krishna, C.V. Navin, S. Biswas, V. Singh, K. Ham, G.L. Bovenkamp, C.S. Theegala, J.T. Miller, J.J. Spivey, C.S.S.R. Kumar. J. Am. Chem. Soc., 135 (2013), pp. 5450-5456.

64. C. Hammond, J.A. Lopez-Sanchez, M. Hasbi Ab Rahim, N. Dimitratos, R.L. Jenkins, A.F. Carley, Q. He, C.J. Kiely, D.W. Knight, G.J. Hutchings. Dalton Trans., 40 (2011), pp. 3927-3937.

65. J.S. Valente, E. Lima, J.A. Toledo-Antonio, M.A. Cortes-Jacome, L. Lartundo-Rojas, R. Montiel, J. Prince. J. Phys. Chem. C, 114 (2010), pp. 2089-2099.

66. S.-P. Li, J.-J. Xu, H.-Y. Chen. Mater. Lett., 59 (2005), pp. 2090-2093.

67. W. Zhao, L. An, S. Wang. Polymers, 13 (2021), p. 296.

68. D. Wang, X. Zhang, X. Cong, S. Liu, D. Zhou. Appl. Catal. A, 555 (2018), pp. 36-46.